JOURNAL OF COMPUTATIONAL PHYSICS **132,** 291–298 (1997)
ARTICLE NO. CP965636

2-D Guiding Centre Simulation of Toroidal Electron Clouds

S. S. Khirwadkar,* P. S. Pathak, S. Chaturvedi, and P. I. John

**Institute for Plasma Research, Bhat, Gandhinagar, 382 428, India*
E-mail: *sameer@plasma.ernet.in

Received July 17, 1995; revised August 9, 1996

A 2-D electrostatic particle simulation code has been developed to study various processes in toroidal electron clouds that occur on time scales much longer than the electron cyclotron period. This code can be applied to gain insight into $k_{\|} = 0$ experimental phenomena encountered in toroidal electron plasmas. Simulation runs have been carried out for model toroidal systems with various aspect ratios. The plasma is observed to reach a steady state which is shifted radially inwards with respect to the minor axis. This inward shift is due to toroidal effects as it is found to increase when the aspect ratio of the torus is decreased. Checks are made to confirm the correct operation of the code and a quantitative comparison of shifts obtained from theory and simulation is presented.

1. INTRODUCTION

Non-neutral, charged clouds trapped in simple magnetic bottles, where the electrostatic repulsion between the charges is balanced by the magnetic force resulting in dynamic equilibrium, have turned out to be excellent test beds for the study of many fundamental properties of confined plasmas. In a series of elegant and thorough experiments, Malmberg and his co-workers [1] have demonstrated the existence of nonneutral plasma equilibria and have investigated various other properties in linear cylindrical devices. These linear devices maintain confinement in the axial direction via electrostatic barriers at the ends of the cylindrical cavities. Toroidal confinement devices, on the other hand, have closed field lines and no potential *plug* is required to achieve axial confinement. The magnetic field lines are, however, curved and this introduces many of the additional features which are absent in the linear cylindrical devices. The dominant drift in both systems is the $\mathbf{E} \times \mathbf{B}$ drift, as a result of which particles move close to the equipotential surfaces. The presence of closed equipotential surfaces in nonneutral systems results in plasma confinement.

The importance of partical simulation codes in understanding various complicated processes has been realised time and again. Many codes have been developed to suit some specific application. One such code has been developed to study the toroidal effects on drift wave turbulance in both linear and non-linear regimes [2]. We have initiated a series of experiments to study the basic properties of low aspect ratio A (A = Major radious R_0/Minor radius a) toroidal electron clouds [3, 4]. The present code has been developed to study the evolution of such a toroidal electron cloud by means of particle simulation. The need for development of such a code was felt because of the difficulty in understanding the complex self consistent motion of electron structures observed in the experiments [4]. The present code can also be utilised to verify the predictions about cloud equilibrium as obtained from equilibrium theories.

In this paper results obtained on using this code to study the effect of toroidicity on the steady state (i.e., near equilibrium) structure of toroidal electron clouds are presented. It is found that in the case of a small aspect ratio torus, the strong toroidicity results in a relatively larger shift of electron cloud structure towards the major axis, consistent with equilibrium theory [5]. The other effects of toroidicity such as elongation and triangularity of the potential profiles has also been observed; however, they will not be discussed in the present paper. The results of simulations carried out for tori having different aspect ratios (see Fig. 1) are presented along with a quantitative comparison of shifts obtained from theory and simulation in large aspect ratio tori.

2. THE CODE

The particle simulation code has three basic structures viz. (1) Particle Pusher; (2) Field Solver, and (3) Information exchanger between particle positions and grid. Various techniques have been developed for each of these structures. One of the earliest particle simulation codes for plasmas in toroidal geometry was developed by C. Z. Cheng and H. Okuda [6].

The crossfield evolution of toroidal electron clouds occurs on time scales much longer than the cyclotron time scale. In order to simulate such slowly evolving processes, the integration of guiding centre equations of motion is always preferable to the integration of exact equations of

0021-9991/97 $25.00

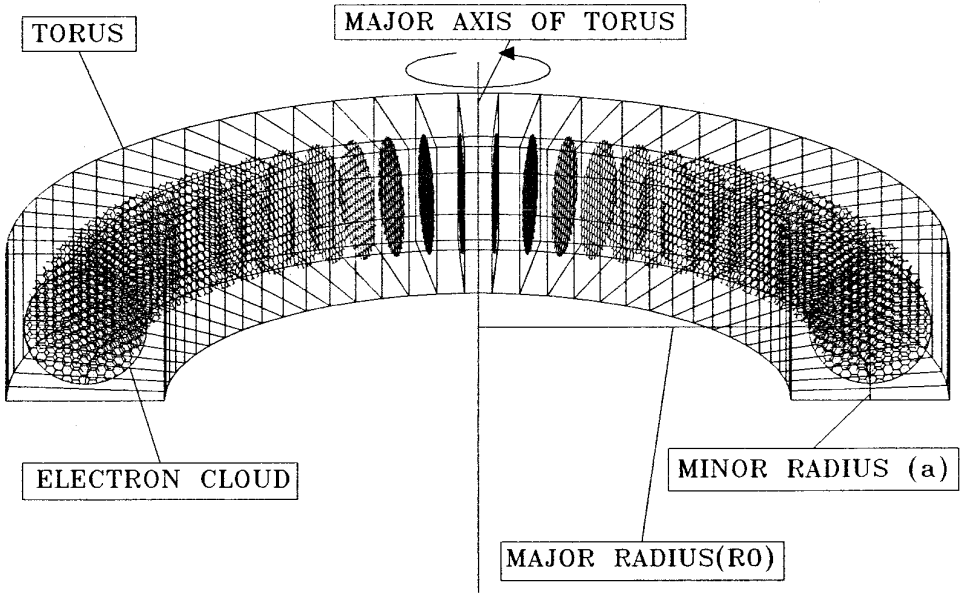

FIG. 1. Schematic diagram of the poloidal cross section of the torus. R_0 = major radius; a = minor radius; A = aspect ratio (R_0/a).

motion because the former requires far less total computation time and yet gives fairly accurate results. There exist various techniques of integration. One of the popular techniques is based on the Monte Carlo scheme. A unified Monte Carlo interpretation of particle simulations and its applications to nonneutral plasmas has been discussed in the paper by A. Y. Aydemir [7]. The present code implements the Predictor-Corrector technique [8] for integration of guiding center equations of motion. The toroidal coordinate is assumed to be an ignorable coordinate and hence the code is basically a two-dimensional code with particles moving in the poloidal plane. This is consistent with the experiments [4] to be analysed as they were performed in a completely toroidally symmetric geometry. Moreover, the use of guiding centre equations of motion for calculation of the particle trajectories can be justified on the following grounds: (1) the scale length of variation of both magnetic and electric field is two orders of magnitude larger than the typical larmour radius, (2) the typical distance covered by the guiding centre in a cyclotron time period is smaller than a larmour radius, and (3) the time scales of phenomena to be analysed are at least three orders of magnitude larger than the electron cyclotron time period.

The values of the various parameters used in this code approximate the experimental situation. For the experiments as well as for the present simulation, it is observed that the major transients in the cloud structure decay on a time scale of 20 μsec. The simulation has been carried out for a total time period of 200 μsec with a time step of 10^{-8} sec.

The code proceeds through a basic cycle as follows: The charge of the particles is first distributed on a 16×16 grid by using a biquadratic spline function for the shape factor of the particles [9]. The charge density is then calculated at the grid points and is used to obtain the electrostatic potential on the same grid via Poisson's equation. The Poisson solver uses the method of Fourier Analysis and Cyclic Reduction (FACR) [10]. The R and Z components of the electric field are obtained at the same grid points, the detailed description of which will be discussed later on. A biquadratic spline interpolation scheme is then used to interpolate the electric field components from grid points to particle locations. This approach of calculating the electric field is different from the method used in [6]. The magnetic field is calculated directly at the particle locations by assuming a purely toroidal magnetic field with radial ($1/R$) dependence (where R is the radial distance from the major axis of torus). The implications of this are discussed later in Section 4. These field quantities are then used to move the particles through one time step by integrating the following nonrelativistic guiding centre equations of motion [11],

$$\dot{\mathbf{R}}_\perp = \frac{\hat{e}_1}{B} \times \left\{ -c\mathbf{E} + \frac{\mu c}{e} \nabla B + \frac{mc}{e} \left[-\mathbf{g} + v_\parallel \frac{\partial \hat{e}_1}{\partial t} + v_\parallel^2 \frac{\partial \hat{e}_1}{\partial s} + v_\parallel \mathbf{u}_E \cdot \nabla \hat{e}_1 + \frac{\partial}{\partial t} \mathbf{u}_E + v_\parallel \frac{\partial}{\partial s} \mathbf{u}_E + \mathbf{u}_E \cdot \nabla \mathbf{u}_E \right] \right\} + O(\varepsilon^2) \tag{1}$$

$$\frac{m}{e}\frac{dv_\parallel}{dt} = \frac{m}{e}g_\parallel + E_\parallel - \frac{\mu}{e}\frac{\partial B}{\partial s} + \frac{m}{e}\mathbf{u}_E \cdot \left(\frac{\partial \hat{e}_1}{\partial t} + v_\parallel \frac{\partial \hat{e}_1}{\partial s} + \mathbf{u}_E \cdot \nabla \hat{e}_1\right) + O(\varepsilon^2) \tag{2}$$

$$\frac{1}{e}\frac{d}{dt}(\textit{kinetic energy}) = \dot{\mathbf{R}} \cdot \mathbf{E}(R,t) + \frac{\mu}{e}\frac{\partial B(R,t)}{\partial t} + O(\varepsilon^2), \tag{3}$$

where c is velocity of light; e and m are the charge and mass of the particle, respectively; $\mathbf{g}$ is the gravitational force; $\hat{e}_1$ and s are the unit vector and distance along the toroidal magnetic field $\mathbf{B}$, respectively; $\dot{\mathbf{R}}_\perp$ is the perpendicular velocity of the guiding centre of the particle; $v_\parallel$ is the velocity of the particle parallel to $\mathbf{B}$; $E_\parallel(E_\perp)$ is the parallel (perpendicular) energy of the particle; μ is the magnetic moment of the particle which is invariant; $\varepsilon = m/e$ is the smallness parameter, and $\mathbf{u}_E = c\mathbf{E} \times \hat{e}_1/B$ is the $\mathbf{E} \times \mathbf{B}$ velocity.

Electric Field Component Calculation Technique. The electric field components in R and Z directions at the particle positions are calculated by using bicubic spline fitting [12]. The potential information available at the grid points is used to fit the bicubic splines along with appropriate boundary conditions. The use of natural cubic splines where the second derivative of potential is assumed to be zero at the two end points of the spline is found to give errors because of the finite grid size. Thus as a first approximation, the charge density very close to the wall is interpolated (by using biquadratic spline interpolation) from the available charge density distribution at the nearby grid points. This interpolated charge density is used as a first approximation to the second derivative of potential at the two ends of the spline. At the radial boundaries $\partial\Phi/\partial z = 0$ and at the Z-boundaries $\partial\Phi/\partial r = 0$ (the tangential components of the electric field), which yields

$$\partial^2\Phi/\partial r^2 = \rho - \frac{1}{r}\partial\Phi/\partial r \tag{4}$$

$$\partial^2\Phi/\partial z^2 = \rho \tag{5}$$

at radial and Z-boundaries, respectively. We will use this property to calculate the second derivative of Φ at the boundary and all over the grid, which will then be used to calculate the electric field components on the grid by the bicubic spline method.

The goal of cubic spline interpolation is to get an interpolation formula that is smooth in the first derivative, and continuous in the second derivative, both within an interval and at its boundaries. This can be written in terms of the second derivative of the function as

$$\Phi = A\Phi_j + B\Phi_{j+1} + C\Phi_j'' + D\Phi_{j+1}'', \tag{6}$$

where A, B, C, and D are defined as

$$A = (r_{j+1} - r)/(r_{j+1} - r_j) \tag{7}$$

$$B = 1 - A = (r - r_j)/(r_{j+1} - r_j) \tag{8}$$

$$C = \tfrac{1}{6}(A^3 - A)(r_{j+1} - r_j)^2 \tag{9}$$

$$D = \tfrac{1}{6}(B^3 - B)(r_{j+1} - r_j)^2 \tag{10}$$

and the derivative of Φ can be written as

$$\frac{d\Phi}{dx} = \frac{\Phi_{j+1} - \Phi_j}{x_{j+1} - x_j} - \frac{3A^2 - 1}{6}(x_{j+1} - x_j)\Phi_j'' + \frac{3B^2 - 1}{6}(x_{j+1} - x_j)\Phi_{j+1}'', \tag{11}$$

where $x = r, z$.

From the condition that the second derivative should be continuous at the grid boundaries, equating Eq. (11) at $x = x_j$ in the interval (x_{j-1}, x_j) and in (x_j, x_{j+1}), this gives (for $j = 2, \ldots, N-1$)

$$\frac{x_j - x_{j-1}}{6}\Phi_{j-1}'' + \frac{x_{j+1} - x_{j-1}}{3}\Phi_j'' + \frac{x_{j+1} - x_j}{6}\Phi_{j-1}'' = \frac{\Phi_{j+1} - \Phi_j}{x_{j+1} - x_j} - \frac{\Phi_j - \Phi_{j-1}}{x_j - x_{j-1}}. \tag{12}$$

These are $N-2$ linear equations in the N unknowns Φ_j'', $j = 1, \ldots, N$. Using the condition that the tangential component of the electric field at the boundary is zero we can get two other equations at the boundaries using Eq. (4),

$$\frac{4x_1 - x_2}{3x_1}\Phi_1'' + \frac{x_1 - x_2}{6x_1}\Phi_2'' = \rho_1 - \frac{\Phi_2 - \Phi_1}{x_1(x_2 - x_1)} \tag{13}$$

and

$$\frac{x_n - x_{n-1}}{6x_n}\Phi_{n-1}'' + \frac{4x_n - x_{n-1}}{3x_n}\Phi_n'' = \rho_n - \frac{\Phi_n - \Phi_{n-1}}{x_n(x_n - x_{n-1})}. \tag{14}$$

For Z-boundaries, Eq. (5) will be used. This set of equations is not only linear, but also *tridiagonal.* Each Φ_j'' is coupled only to its nearest neighbour at $j \pm 1$. Solving these equations will yield the second derivative of Φ in the respective directions, which will then be used by other

TABLE I

Aspect ratio	Inner wall radius Rin(cm)	Outer wall radius Rout(cm)	Z-height Z(cm)	Total charge Q(StC)	Total particles N	Magnetic field B_0(Gauss)	Time step $\Delta t(\mu s)$	Maximum time Tmax(μs)
5	35.0	52.5	17.5	30.0	1369	500	0.01	200
100	866.25	883.75	17.5	600.0	1369	500	0.01	200

routines for the calculation of electric field components at the grid points.

3. IMPLEMENTATION

The code has been implemented to study the evolution of electron cloud in tori having aspect ratios in the range from 1.5 to 100, all with the identical square poloidal cross section of side 17.5 cm. An equipotential boundary with the boundary potential $\Phi_{Boundary} = 0$ is assumed. In the following discussion, the cases with aspect ratios of 5 and 100 (named as T5 and T100, respectively) are discussed in greater detail than the others.

There are two reasons for choosing these particular aspect ratios. Firstly, the theory that is used for comparison of the result for radial shift in the equilibrium position of the electron cloud due to toroidal effect is valid for large aspect ratios only. Secondly, since the radius of curvature of toroidal magnetic field lines in T5 is 20 times smaller than those in T100, comparison of the results for T5 and T100 can show the effect of toroidicity on the properties of the electron cloud. Moreover, since the gradient of toroidal magnetic field has $(1/R^2)$ dependence, T100 has a gradient which is 400 times less than that for T5, i.e., the magnetic field in T100 is approximately uniform across the poloidal cross section. Thus the large radius of curvature and the small magnetic field gradient in T100 can allow us to compare the result with the experimental results in the popular Malmberg Traps which are linear cylindrical devices with uniform magnetic field.

To validate the code, the particles are also moved using the $\mathbf{E} \times \mathbf{B}$ drift alone. In this case, the particle motion should be confined to the equipotential surfaces and since these surfaces are concentric in nature for the equipotential boundary condition, there should be absolute conservation of total energy and total number of particles.

The input parameters are given in the Table I, where B_0 is the magnetic field at the minor axis, StC is the charge in Stat-Coulomb, Z-height is the vertical extent of the torus (parallel to the major axis) and the midplane of the torus is at Z = (Z-height/2) = 8.75 cm. The total charge has been chosen so as to keep the charge density $\simeq 3.56 \times 10^{-4}$ StC/cc, the same for both aspect ratios.

The particles are initially loaded into the torus as described below: The total charge Q confined in the torus is divided equally among a total of N simulation particles. The particles are distributed uniformly in a circular region around the minor axis with radius slightly smaller than the minor radius (a) of the torus. The parallel energy of particles $E_\parallel$ is assumed to be zero. The perpendicular energy $E_\perp$ is given by the particle magnetic moment μ which is chosen so as to yield an $\exp(-\mu/\mu_0)$ type of distribution, where μ_0 ($=E_\perp/B_0$) is the magnetic moment of a particle at the minor axis having $E_\perp = 10\,eV$. For numerical convenience, the value of μ is restricted to lie between $\mu_0/2$ and $2 \times \mu_0$.

The guiding center equations of motion are based on the assumption of the invariance of magnetic moment of charged particles (Eqs. (2), (3)). Thus, when a particle experiences change in the background magnetic field, its perpendicular kinetic energy also changes in such a way that the magnetic moment of the particle remains unaltered. This property has been used to calculate the perpendicular velocity ($v_\perp$) of particles which is later used to calculate the drifts related to $v_\perp$.

The particle trajectories are followed by assuming the particles to be electrons. However, since a small number of simulation particles are representing a large number of electrons, the particles are appropriately weighted while calculating the electric field and total system energy.

4. RESULTS

Table II shows a comparison of energy and particle loss between simulation runs carried out for particle motion exclusively with $\mathbf{E} \times \mathbf{B}$ drift alone and with inclusion of all guiding centre drifts.

TABLE II

No.	Torus	Allowed drifts	Total charge loss (%)	Total energy deviation (%)
1	T5	$\mathbf{E} \times \mathbf{B}$ alone	−0.80	−0.070 to 0.007
2	T5	All drifts	−2.41	−0.170 to 0.007
3	T100	$\mathbf{E} \times \mathbf{B}$ alone	0.0	−0.020 to 0.020
4	T100	All drifts	0.0	−0.020 to 0.030

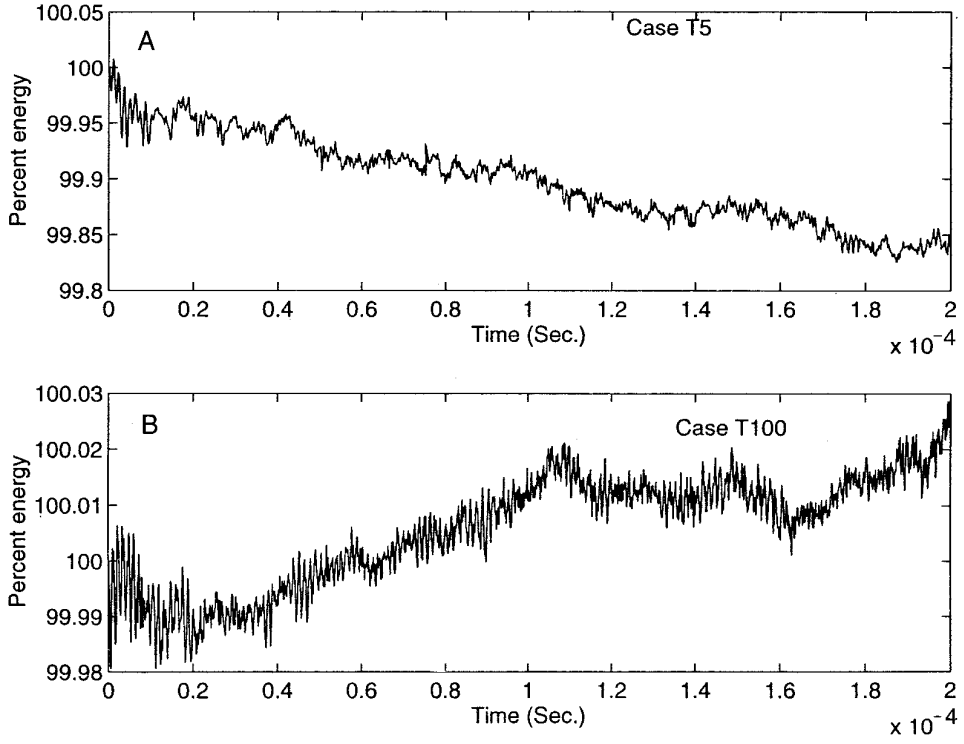

FIG. 2. Percentage variation of total energy (relative to the initial total energy) with time. (A) Total energy for T5; (B) total energy for T100.

A study of Table II shows the following features:

(1) There is no charge loss until 200 μsec for T100 where the magnetic field gradient is weak.

(2) In the T5 case, the charge loss with $\mathbf{E} \times \mathbf{B}$ alone is 66% less than that for the case with all drifts. Thus, the confinement of particles is much better if only $\mathbf{E} \times \mathbf{B}$ drift is allowed.

(3) In the T5 case, the energy loss with $\mathbf{E} \times \mathbf{B}$ alone is 59% less than that for the case with all drifts. Thus, the energy confinement is much better if only $\mathbf{E} \times \mathbf{B}$ drift is allowed.

(4) In the T100 case, the energy and particle loss is almost the same for both cases of $\mathbf{E} \times \mathbf{B}$ alone and all drifts allowed. This indicates that $\mathbf{E} \times \mathbf{B}$ drift is the only dominant drift in T100, as $\mathbf{B}$ is almost uniform.

(5) The positive deviation in total energy cannot be explained since there is no source which can pump extra energy into the system. Thus this deviation is purely due to computational inaccuracy.

The computational inaccuracy mentioned above can arise because of several reasons such as (a) a small number of simulation quasi-particles representing a large number of actual particles. (b) Particles are not moved continuously in time; they move with finite time step (jump). (c) The discrete information about charge or potential distribution on a finite grid is used to solve the Poisson equation. (d) The discrete information about electric field components available on the grid is interpolated at the particle location for calculation of various drifts.

Figure 2 shows the variation of total energy with time for T5 and T100 for the case where particle motion includes all guiding centre drifts. The total energy (including the kinetic energy of particles lost to system walls) is conserved to better than 0.17% in case of T5 (Fig. 2A) and better than 0.02% in case of the T100 torus (Fig. 2B). At the end of 200 μsec, no particle loss is observed in T100, whereas around 2.41%, loss of particles is observed in T5 (see Fig. 3). The particle loss to the boundaries is found to increase with a decrease in the aspect ratio of the torus, i.e., increase in ∇B and increase in $E_\perp$ of particles. In the T5 case, ∇B drift is two order larger than the other drifts (excluding $\mathbf{E} \times \mathbf{B}$ drift, which is two order larger than ∇B drift), while in the T100 case this ratio is of one order. This shows that ∇B drift is one of the mechanisms for particle loss to the walls.

If the equations involve a purely $\mathbf{E} \times \mathbf{B}$ drift then the particles would simply move along equipotential surfaces. In the case of an equipotential boundary ($\Phi_{boundary} = 0$), equipotential contours would never intersect the wall and

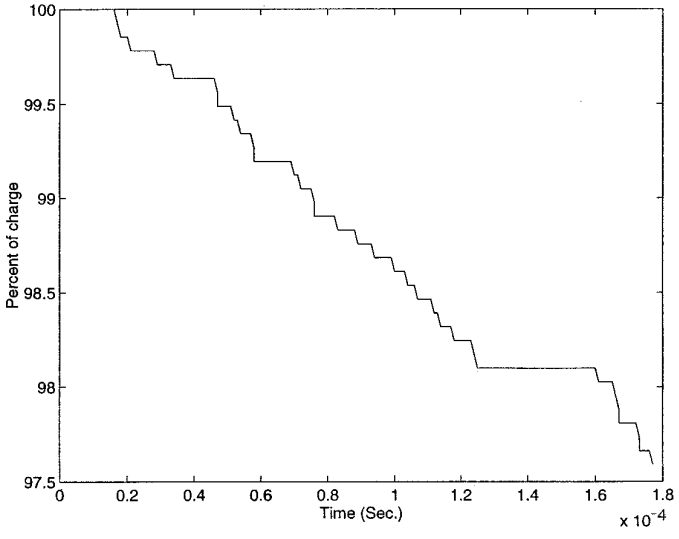

FIG. 3. Percentage loss of total charge (relative to the initial total charge) with time.

hence ideally there would be no particle loss. However, when higher order drifts are included (as in our study), particles can have excursions about the equipotential surfaces.

The electric field is first calculated on the grid points by using bicubic spline interpolation and then calculated at the particle position by biquadratic spline interpolation from nearby grid points. The magnetic field is however calculated directly at the particle position by using $(1/R)$ dependence. This is done because the biquadratic spline interpolation of magnetic field from grid points on the particle location shows poor conservation results (Table III) as compared to those for direct calculation (Table II).

In Table III, the subscript ''quad'' implies that the toroidal magnetic field at the particle location is calculated by using biquadratic spline interpolation.

The comparison between initial ($t = 0$ μsec) and final ($t = 200$ μsec) equipotential contours is shown in Fig. 4. As can be seen here, the initial and final cloud structures are almost the same in case of T100, whereas in the case of T5, the final structure is shifted radially inward with respect to the initial structure.

TABLE III

No.	Torus	Allowed drifts	Total charge loss (%)	Total energy deviation (%)
1	T5	$\mathbf{E} \times \mathbf{B}_{quad}$ only	−1.30	−0.080 to 0.007
2	T5	All_{quad} drifts	−2.70	−0.190 to 0.007
3	T100	$\mathbf{E} \times \mathbf{B}_{quad}$ only	0.0	−0.020 to 0.030
4	T100	All_{quad} drifts	0.0	−0.020 to 0.010

The global motion of the electron cloud is observed by monitoring the temporal evolution of centre of charge (R_c, Z_c) in poloidal cross-section of the torus. Here R_c and Z_c are defined as $R_c = \Sigma_{i=1}^{N} R_i \times Q_i/Q_{total}$ and $Z_c = \Sigma_{i=1}^{N} Z_i \times Q_i/Q_{total}$. The Centre of Charge (COC) is observed to *spiral in* towards an equilibrium position at the centre of the spiral. The inward spiral motion of COC is more marked in low aspect ratio cases as compared to high aspect ratio cases. This can be understood as follows: In all cases, the simulation was started with the particle distribution symmetric around the minor axis of the torus so that the distance of COC from the minor axis of torus is $(\Delta_R = 0, \Delta_z = 0)$. Such a distribution of particles is one of the equilibrium positions of the COC for cylindrical electron clouds $(A \to \infty)$. The T100 case is an approximation to the cylindrical limit hence little spiralling is expected. On the other hand, the equilibrium position of the COC for T5 is expected to be greatly shifted relative to the minor axis, hence a larger circle radius is expected in the initial stages which should decay in time. At large times, the trajectory of COC is nearly circular and the centre of this circle is shifted with respect to the minor axis by amounts Δ_R and Δ_Z in the R and Z directions.

The shifts (Δ_R, Δ_Z) are found to be (−1.0 cm, −0.05 cm) and (−0.05 cm, −0.01 cm) for T5 and T100, respectively. The small value of Δ_Z/Δ_R in T5 as well as T100 indicates that the steady state cloud structure is more or less symmetric around the midplane of the torus. The difference in Δ_R values for T5 and T100 shows the effect of toroidicity on the equilibrium structure of toroidal electron clouds.

Theoretical estimates of Δ_R in the large aspect ratio limit could be obtained from the following expression [5],

$$\frac{d\Delta}{dr} = \frac{1}{rR_0\Phi_0'^2}\int_0^r \Phi_0'^2 r\,dr + \frac{r}{R_0}, \tag{15}$$

where $\Delta_R = \Delta_{r=0}$, r is the distance from the minor axis of the torus, R_0 is the major radius of the torus, $\Phi_0(r)$ is the lowest order (cylindrical) approximation of potential distribution, and $\Phi_0' = d\Phi_0/dr$. In order to calculate the shift, a parabolic potential profile $\Phi_0(r) = \Phi_0(r^2/a^2 - 1)$ has been assumed which is the solution for potential $\Phi_0(r)$ in case of a straight circular cylinder with uniform electron density. In the limit of $r \to 0$ and using $\Delta_{r=a} = 0$ as a boundary condition, the above expression reduces to a simple equation for shift: $\Delta_{r=0} - (5/8)\varepsilon a$.

The shifts obtained from simulations carried out for tori having different aspect ratios are shown in Fig. 5 along with the shifts obtained from the above equation for large aspect ratio torus. A close agreement has been observed in shift for aspect ratio (A) greater than 5. The theoretical shifts are not calculated for low aspect ratio tori because of the inapplicability of theory in that regime.

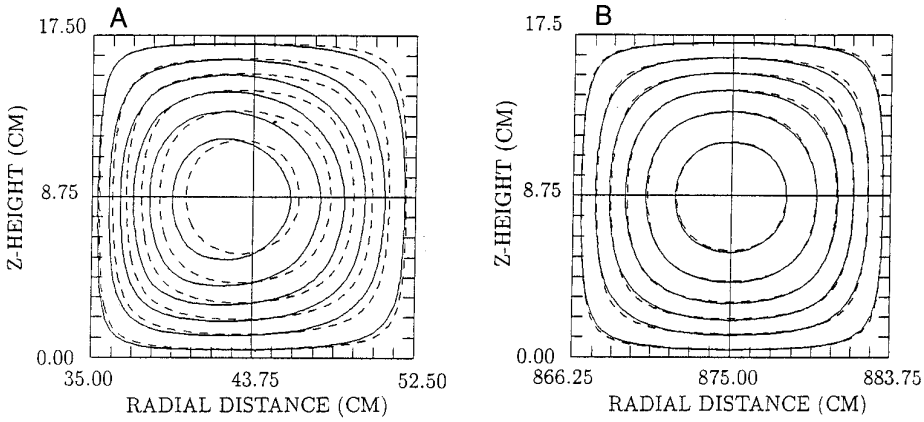

FIG. 4. The comparison between initial (dashed contours) and final equipotential contours for (A) T5 and (B) T100 torus. The inward shift of cloud in case of T5 shows the effect of toroidicity on the steady state structure of the toroidal electron cloud.

5. CONCLUSIONS

We have developed a 2-D particle simulation code to study the properties of toroidal electron clouds. In the case of the torus having aspect ratio 5 (100), better than 0.17% (0.02%) conservation of total energy throughout the 20,000 time steps of simulation verifies the proper functioning of the code. The reasons for observed increase in particle losses to the walls with a decrease in the aspect ratio of the torus have not yet been identified. However, the observation of increase in particle loss with a decrease in the aspect ratio of the torus and an increase in perpendicular energy of particles suggests that ∇B drift, which is a dominant drift, is one of the mechanisms for particle loss to the walls.

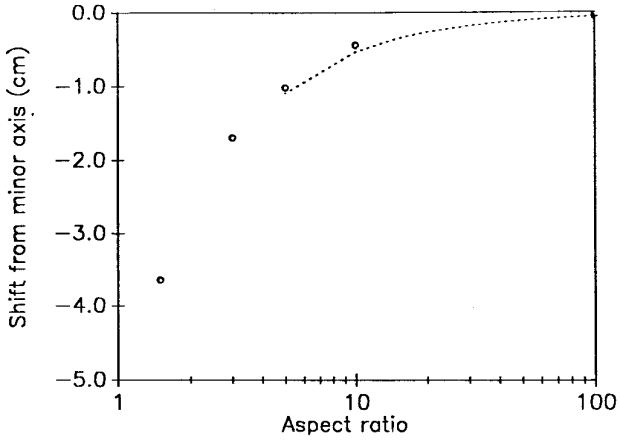

FIG. 5. Dependence of radial shift in the centre of the charge on the aspect ratio of the torus. The dotted line represents theoretical values and circles represent computational values.

The implementation of the code to study the effect of toroidicity on steady state structures of toroidal electron clouds has shown an inward shifted equilibrium which is qualitatively in agreement with theory. A quantitative comparison shows a close agreement between shifts obtained from theory and simulation for large aspect ratio tori. The difference in shifts can be due to the following reasons: Firstly, the theory has been developed explicitly for equilibrium of cold electrons confined in large aspect ratio torus and hence its application to the case of warm electrons confined in a low aspect ratio torus is subject to errors. Secondly, the parabolic potential profile for $\Phi_0(r)$ is an assumption which is used to simplify the calculations for shift whereas the actual potential profiles in simulation are not necessarily parabolic. The simulation result itself is subject to some additional errors because of the use of a coarse (16×16) grid for solving Poisson's equation and the use of a very small number of particles ($N = 1369$) each representing as many as 10^8 electrons.

The present code will be used in the future to explore various properties of toroidal electron clouds. The future work includes implementation of the code to: (1) simulate near experimental conditions to gain a better understanding of the experimentally observed process of toroidal electron cloud formation; (2) simulate the conditions assumed by the theoretical models so as to verify theoretical predictions about cloud equilibrium; and (3) study the different stable and unstable modes existing in the torus.

ACKNOWLEDGMENTS

We are grateful to Dr. H. Ramachandran for useful discussions during development of this simulation code and for valuable comments during the writing of this paper. We are also grateful to Dr. K. Avinash for useful discussions on equilibrium theory of toroidal electron clouds.

REFERENCES

1. J. H. Malmberg *et al.*, in *Proc. AIP Conference On Non Neutral Plasmas,* edited by C. W. Roberson and C. F. Driscall (Am. Inst. of Phys., New York, 1988).
2. M. J. LeBrun *et al.*, *Phys. Fluids B* **5,** 752 (1993).
3. P. Zaveri *et al.*, *Phys. Rev. Lett.* **68,** 3295 (1992).
4. S. S. Khirwadkar *et al.*, *Phys. Rev. Lett.* **71,** 4334 (1993).
5. K. Avinash, *Phys. Fluids B* **3,** 3226 (1991).
6. C. Z. Cheng and H. Okuda, *J. Comput. Phys.* **25,** 133 (1977).
7. A. Y. Aydemir, *Phys. Plasmas* **1,** 822 (1994).
8. W. W. Lee and H. Okuda, *J. Comput. Phys.* **26,** 139 (1978).
9. C. K. Birdsall and A. B. Langdon, *Plasma Physics via Computer Simulation* (McGraw–Hill, New York, 1985).
10. M. H. Hughes, *Comput. Phys. Commun.* **2,** 157 (1971).
11. T. G. Northrop, *Adiabatic Motion of Charged Particles,* edited by E. Marshak (Interscience, New York, 1963).
12. W. H. Press *et al.*, *Numerical Recipes in FORTRAN: The Art of Scientific Computing,* 2nd ed. (Cambridge Univ. Press, New Delhi, 1992).